Evolution of the Local Structure around Ti Atoms in $NaAlH_4$ Doped with $TiCl_3$ or Ti_{13}·6THF by Ball Milling Using X-ray Absorption and X-ray Photoelectron Spectroscopy

Aline Léon,*,† Oliver Kircher,† Maximilian Fichtner,† Jörg Rothe,‡ and Dieter Schild‡

Institut für Nanotechnologie and Institut für Nukleare Entsorgung, Forschungszentrum Karlsruhe GmbH, P.O. Box 36 40, 76021 Karlsruhe, Germany

Received: September 9, 2005

X-ray absorption and X-ray photoelectron spectroscopy are used to investigate $NaAlH_4$ doped with 5 mol % of Ti on the basis of either $TiCl_3$ or Ti_{13}·6THF by ball milling. X-ray photoelectron spectroscopy (XPS) analysis of $TiCl_3$ or Ti colloid doped samples indicates that Ti species do not remain on the sample surface but are driven into the material with increasing milling time. The surface concentration of Ti continues to decrease during subsequent cycles under hydrogen. After several cycles, it reaches a constant value of 0.5 at. % independently of the nature of the precursor. Moreover, metallic aluminum is already present at the surface after 2 min of ball milling in the case of $TiCl_3$ doped Na-alanate, whereas it is totally absent in the case of Ti colloid doped samples at any milling time. Upon cycling, the atomic concentration of metallic Al at the surface evolves with the reaction under hydrogen, in contrast to the Ti concentration. Analysis of the binding energies of samples doped with $TiCl_3$ or Ti colloid, after eight desorption/absorption cycles, reveals that the Na, O, and Ti environment remains the same, while the Al environment undergoes changes. According to the extended X-ray absorption fine structure (EXAFS) analysis of $TiCl_3$ doped Na-alanate, the local structure around Ti during the first cycle is close to that of metallic Ti but in a more distorted state. In the case of the Ti colloid doped sample, a stripping of the oxygen shell occurs. After eight cycles, a similar intermetallic phase between Ti and Al is present in the hydrogenated state of $TiCl_3$ or Ti colloid doped samples. The local structure around Ti atoms after eight cycles consists of Al and Ti backscatterers with a Ti−Al distance of 2.79 Å and a Ti−Ti distance of 3.88 Å. This local structure is not exactly the $TiAl_3$ phase because it differs significantly from the alloy phase in its fine structure and lacks long-range order. Volumetric measurements performed on these samples indicate that the formation of this local structure is responsible for the reduction of the reversible hydrogen capacity with the increasing number of cycles. Moreover, the formation of the alloy-like phase is correlated with a decrease of the desorption/absorption reaction rate.

1. Introduction

Hydrogen can be stored as a compressed gas, as a cryogenic liquid, or in the form of chemical compounds, such as metal hydrides. When using this latter form, many limitations that are encountered with compressed or liquid hydrogen are avoided, such as high storage pressure, low temperature, and high loss of vaporized hydrogen. However, use of such storage systems in mobile applications will depend on identifying a material that fulfils several prerequisites, e.g., among others, a reversible hydrogen storage capacity close to 6 wt %, a refuelling time of less than 5 min, and an ideal operating temperature range between 80 and 100 °C.

Of the complex metal hydrides, the system that presently is the most promising one is sodium aluminum hydride, or sodium alanate, $NaAlH_4$. Its decomposition takes place in three steps according to the following reactions:

$$3NaAlH_4 \rightleftarrows Na_3AlH_6 + 2Al + 3H_2 \quad (1)$$

$$Na_3AlH_6 \rightleftarrows 3NaH + Al + {}^3/_2H_2 \quad (2)$$

$$3NaH \rightleftarrows 3Na + {}^3/_2H_2 \quad (3)$$

Without taking into account the third step occurring at temperatures higher than 400 °C, the decomposition of the pure alanate leads to a hydrogen storage capacity of 5.6 wt % (cf. Figure 1). Unfortunately, the kinetics of the pure material is not favorable for practical applications.

A breakthrough in the thermodynamic and kinetic properties of this material has been achieved by adding a metal precursor to the alanate.[1] With the doped material, the decomposition and backward reaction take place below the melting point. Moreover, the conditions required to reach a reasonable driving force for the reaction and usable kinetics are drastically reduced compared to pure alanate. Of these precursors, $TiCl_3$ and Ti_{13}·6THF have appeared to be the most efficient ones in terms of kinetics and hydrogen storage capacity when added to the alanate. The kinetics of the decomposition reaction of pure sodium alanate and that of sodium alanate doped with 5 mol % of Ti on the basis of $TiCl_3$ or Ti_{13}·6THF are compared in Figure 1. The decomposition of purified $NaAlH_4$ that has been ball milled for 30 min and held at 170 °C results in the release of the theoretical amount of 5.6 wt % of hydrogen. The decomposition of the doped material is highly dependent on the nature of the dopant.

* Dr. Aline Léon Institut für Nanotechnologie, Forschungszentrum Karlsruhe GmbH, P.O. Box 36 40, 76021 Karlsruhe, Germany. Tel: (+49) 7247/82-6778. Fax: (+49) 7247/82−6368. E-mail: aline.leon@int.fzk.de.
† Institut für Nanotechnologie.
‡ Institut für Nukleare Entsorgung.

10.1021/jp055100b CCC: $33.50
Published on Web 12/27/2005

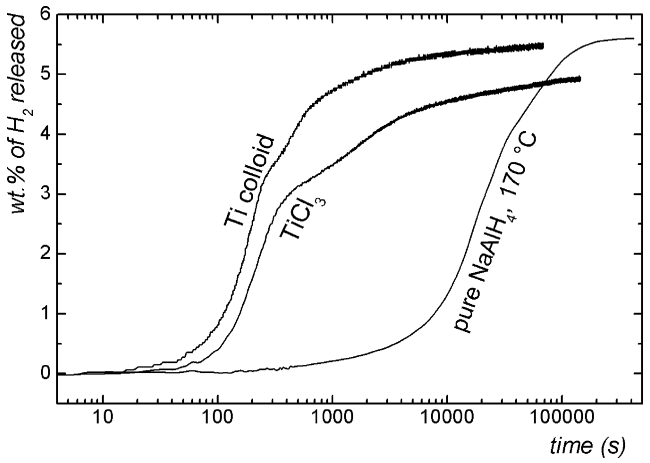

Figure 1. Isothermal decomposition kinetics of the first desorption of pure $NaAlH_4$ held at 170 °C and of Na-alanate doped with 5 mol % of Ti on the basis of $TiCl_3$ or Ti_{13}·6THF held at 150 °C under a residual hydrogen pressure of 0.3 bar.

In fact, 4.5 wt % of H_2 is released within 700 s from sodium alanate doped with Ti colloid, whereas 8000 s are needed to reach this state of the reaction when using the $TiCl_3$ doped sample. The differences between the three materials are drastic. In addition to differences in kinetics, the reversible hydrogen storage capacities differ as well. The reason for this difference is not clear at present.

Several characterization methods (X-ray diffraction (XRD),[2,3] PND,[4,5] scanning electron microscopy/transmission electron microscopy (SEM/TEM),[6−9] X-ray absorption spectroscopy (XAS),[8,10,11] and X-ray photoelectron spectroscopy (XPS)[12]) have been applied to understand the role of titanium when added to $NaAlH_4$. The chemical state of Ti has been clarified,[8,10,11] but the nature of the Ti phase present in the Ti doped $NaAlH_4$ system is still a matter of discussion. Moreover, questions concerning the physical mechanism of enhanced kinetics upon doping with Ti are unanswered. An understanding of the differences observed with these two precursors may give hints concerning the mechanism involved in the absorption and desorption of hydrogen in doped sodium alanate. This, in turn, may allow for an optimization of the kinetic properties by modifying the nature of the precursors.

The aim of this work is to correlate experimental data of processes occurring in the material with the observed kinetics and the storage capacity (cf. Figure 1) of Na-alanate samples doped with $TiCl_3$ or Ti_{13}·6THF precursors. For this purpose, XPS and XAS have been applied to study the behavior of titanium atoms at the surface and in the bulk material upon milling and subsequent cycling. Na-alanate doped with 5 mol % of Ti on the basis of Ti_{13}·6THF or $TiCl_3$ has been prepared using different milling times (2, 30, 60, and 180 min) and different decomposition/absorption cycles (during the first cycle, after the first cycle, and after eight cycles). Then, the respective samples have been investigated. To complete the results obtained from XPS and extended X-ray absorption fine structure (EXAFS) analysis, dehydrogenation and hydrogenation kinetics of these samples will be presented.

2. Experimental Section

2.1. Sample Preparation. All sample preparations were done in an argon-filled glovebox equipped with a recirculation system to keep the water and oxygen concentrations below 1 ppm. Chemical operations were performed on the bench under purified nitrogen using Schlenk tube techniques.

TABLE 1: Sample Description

label	sample description
Ti	Ti metallic foil
$TiCl_3$	$TiCl_3$ as received (99.999%, Sigma Aldrich)
Ti_{13}·6THF	Ti_{13}·6THF as synthesized (purity of 74%)
$TiAl_3$	Ti/Al alloy as received (99.5%, Alfa Aesar)
TiH_2	TiH_2 as received (99%, Alfa Aesar)
(bm2)	$NaAlH_4$ + 5 mol % of Ti on the basis of $TiCl_3$ or Ti_{13}·6THF, ball milled 2 min at 600 rpm
(bm30)	$NaAlH_4$ + 5 mol % of Ti on the basis of $TiCl_3$ or Ti_{13}·6THF, ball milled 30 min at 600 rpm
(bm60)	$NaAlH_4$ + 5 mol % of Ti on the basis of $TiCl_3$ or Ti_{13}·6THF, ball milled 60 min at 600 rpm
(bm180)	$NaAlH_4$ + 5 mol % of Ti on the basis of $TiCl_3$ or Ti_{13}·6THF, ball milled 180 min at 600 rpm
(dd)	$NaAlH_4$ + 5 mol % of Ti on the basis of $TiCl_3$ or Ti_{13}·6THF, ball milled 30 min and quenched once 2.6 wt % H_2 is released[a]
(a1d)	$NaAlH_4$ + 5 mol % of Ti on the basis of $TiCl_3$ or Ti_{13}·6THF, ball milled 30 min and stopped after the 1st desorption[a]
(da)	$NaAlH_4$ + 5 mol % of Ti on the basis of $TiCl_3$ or Ti_{13}·6THF, ball milled 30 min and quenched once 2.3 wt % H_2 is absorbed[b]
(a1a)	$NaAlH_4$ + 5 mol % of Ti on the basis of $TiCl_3$ or Ti_{13}·6THF, ball milled 30 min and stopped after the 1st absorptiojn[b]
(a2a)	$NaAlH_4$ + 5 mol % of Ti on the basis of Ti_{13}·6THF, ball milled 30 min and stopped after the 2nd absorption[b]
(a8a)	$NaAlH_4$ + 5 mol % of Ti on the basis of $TiCl_3$ or Ti_{13}·6THF, ball milled 30 min and stopped after 8th absorption[b]
(a9d)	$NaAlH_4$ + 5 mol % of Ti on the basis of $TiCl_3$ or Ti_{13}·6THF, ball milled 30 min and stopped after 9th desorption[a]

[a] T = 150 °C, p_{H_2} = 0.3 bar. [b] T = 100 °C, p_{H_2} = 100 bar.

Commercially available $NaAlH_4$ (Chemetall, Frankfurt) was purified by a Soxhlet extraction with THF as described in ref 13. The samples doped with a Ti-based catalyst were prepared using either $TiCl_3$ (99.999%, Sigma Aldrich) or Ti_{13}·6THF.[13] According to elemental analysis, Ti_{13}·6THF contained 44 wt % of Ti, 1.4 wt % of B, and 7.9 wt % of K.

In an argon glovebox, a silicon nitride vial containing balls made of the same material was filled with either 285 mg of $TiCl_3$ or 513 mg of Ti_{13}·6THF product and 2 g of purified sodium alanate and sealed. The ball to powder weight ratio was about 20:1, and milling was carried out in a Fritsch P6 planetary mixer/mill.

Absorption and desorption of hydrogen were carried out in a modified Sieverts apparatus. A more detailed description of the apparatus, the reactor, and the measurement procedure can be found in refs 13 and 14.

Investigation concentrated on the evolution of the local structure around Ti in samples quenched at a defined degree of the dehydrogenation−rehydrogenation reaction (cf. Table 1). Moreover, $TiAl_3$ alloy (99.999%, Alfa Aesar) and TiH_2 (99.999%, Alfa Aesar) (cf. Table 1) were analyzed.

2.2. X-ray Absorption Spectroscopy (XAS). X-ray absorption spectroscopy was performed on the samples at the Ti K-edge (4966 eV). The measurements were carried out at the ANKA-XAS beamline, Forschungszentrum Karlsruhe, Germany. The Ti K-edge X-ray absorption spectrum of a Ti metal foil was measured for energy calibration in the transmission mode. Ti metal was also used as a reference sample. $TiCl_3$, Ti_{13}·6THF, $TiAl_3$, and TiH_2 were measured in the transmission mode. Due to the low concentration of Ti in the doped sodium alanate samples, these spectra were taken in the fluorescence mode at room temperature, with the Ti K_α radiation (∼4510 eV) being

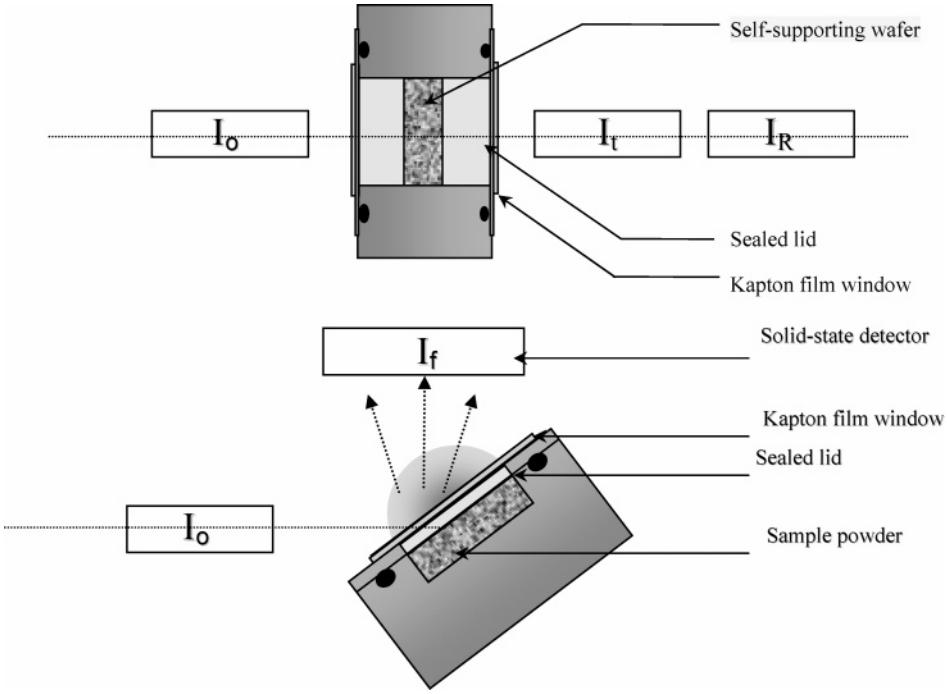

Figure 2. Sample holders used in the transmission mode, a, and the fluorescence mode, b.

collected by a solid-state detector (5-element Canberra LEGe). For the transmission mode, an appropriate amount of powder (optimized to give an absorbance step of one:

$$(\mu x)_{\text{at K-edge}} - (\mu x)_{\text{before K-edge}} = 1$$

where μ is the absorption coefficient and x is the thickness of the sample) was mixed with polyethylene. As shown in Figure 2a, the resulting powder was pressed into a sample holder to produce a self-supporting wafer and sealed with Kapton film windows (thickness of 0.02 mm). For the fluorescence mode, Figure 2b, the cavity was filled with the powder mixed with polyethylene and sealed with Kapton film windows. The sample holders used allowed the samples to be prepared, transferred, and measured without exposing them to air. Spectra were recorded at a step width of 5 eV in pre-edge region 1 (4816−4916 eV), of 2 eV in pre-edge region 2 (4916−4946 eV), of 0.5 eV at the rising edge (4946−5006 eV), and at equidistant k-steps (0.03 $Å^{-1}$) in the post-edge region (5006 − 5941 eV). Up to nine scans were averaged to improve the signal-to-noise ratio. EXAFS (extended X-ray absorption fine structure) data analysis was based on standard least-squares fit techniques,[15] using the UWXAFS[16] program package. A detailed description of the background removal, the normalization procedure, the Fourier transformation, and the fitting procedure can be found in ref 10.

2.3. X-ray Photoelectron Spectroscopy (XPS). For XPS analysis, the powder samples were pressed onto In-foil and mounted on the sample holder. By means of a transfer vessel, samples were transferred from the glovebox to the XPS instrument without exposing them to air. XPS measurements were carried out under an ultimate pressure of 7×10^{-8} Pa with a PHI 5600ci spectrometer (Physical Electronics Inc.) equipped with a hemispherical capacitor analyzer and a multichannel detector. XPS spectra were recorded using Mg Kα (1253.6 eV) or monochromatic Al Kα (1486.6 eV) X-ray sources. High-resolution scans of elemental lines were acquired at a pass energy of 11.75 eV of the analyzer, which yielded a full-width-at-half-maximum (FWHM) value of the Ag $3d_{5/2}$ line of 0.85 and 0.62 eV, respectively. The energy scale of the spectrometer was calibrated with the Cu $2p_{3/2}$, Ag $3d_{5/2}$, and Au $4f_{7/2}$ lines of pure and Ar^+ sputtered cleaned metal foils.[17] The angle of emission (the angle between the analyzer direction and the sample surface normal) was 25° for all measurements. The spectrometer was calibrated such that the standard deviation of binding energies was within ± 0.1 eV for conductors and within ± 0.15 eV for non-conducting samples.

3. Results and Discussion

3.1. Isothermal Decomposition and Absorption Kinetics. $NaAlH_4$ doped with 5 mol % of Ti from Ti_{13}.6THF was decomposed directly after ball milling (milling time 30 min), followed by eight absorption/decomposition cycles. Decomposition measurements were performed at 150 °C under a residual hydrogen pressure of 0.3 bar; those for absorption were done at 100 °C under a hydrogen pressure of 100 bar.

Figure 3 shows the amount of hydrogen released with desorption time for the first and the ninth dehydrogenation cycle of samples (bm2), (bm30), (bm180). As can be seen, 5 wt % of H_2 is released in the first desorption cycle within 500, 2000, and 10 000 s for samples (bm180), (bm30), and (bm2), respectively. The difference in the desorption times of samples (bm180) and (bm30) mainly results from the kinetics of the second step of the reaction, which are slower in sample (bm30) than in sample (bm180). In the subsequent cycles, the kinetics of both samples decreases, and from the fourth cycle, the desorption kinetics do not change significantly. For all samples, 5.5 wt % of H_2 is released after the first decomposition. Then, the storage capacity decreases continuously and reaches a value of 4.5 wt % of H_2 after 4 cycles for samples (bm180) and (bm30) (not shown in Figure 3). As can be observed in Figure 3, the decrease in the hydrogen storage capacity is mainly due to the decrease in the amount released from the first decomposition step (reduction from 3.5 to 2.5 wt %).

Figure 4 displays the absorption curves of the first cycle for sample (bm2) and those of the first and ninth absorption cycles for samples (bm30) and (bm180). As for the desorption, the

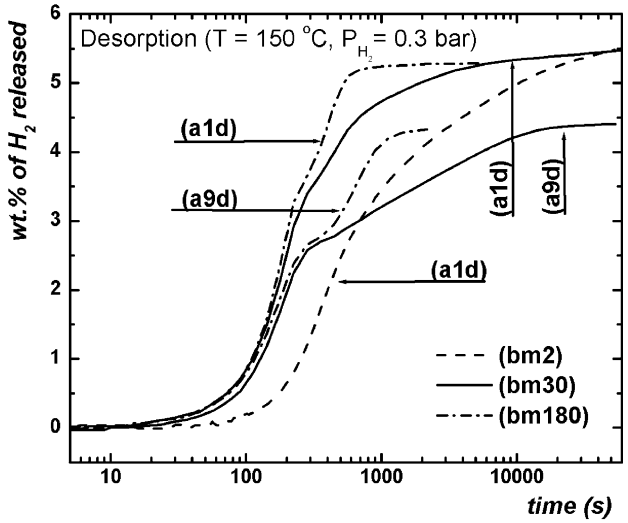

Figure 3. Desorption kinetics of Na-alanate doped with 5 mol % of Ti on the basis of Ti_{13}·6THF at 150 °C under a residual pressure of 0.3 bar of hydrogen. The first and ninth cycles are presented for samples (bm30) and (bm180). Only the first cycle is shown for sample (bm2).

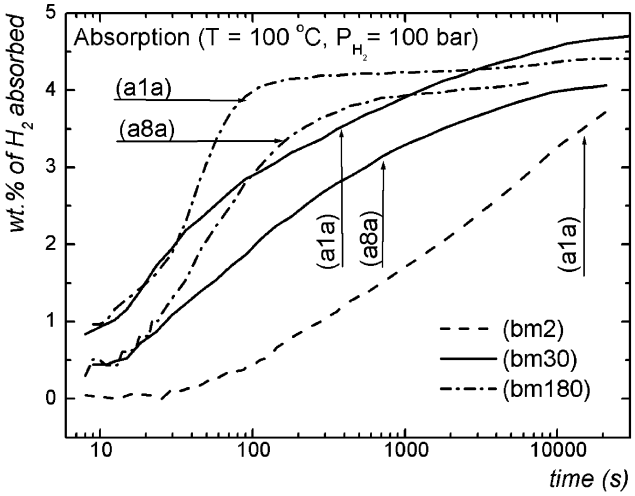

Figure 4. Kinetics of the absorption of Na-alanate doped with 5 mol % of Ti on the basis of Ti_{13}·6THF at 100 °C under a hydrogen pressure of 100 bar. The first and ninth cycles are presented for samples (bm30) and (bm180). Only the first cycle is shown for sample (bm2).

kinetics of absorption is faster for sample (bm180) than sample (bm30). In the first cycle, sample (bm180) has absorbed 3.5 wt % of H_2 within 60 s, whereas sample (bm30) has absorbed 2.5 wt % only. The absorption kinetics and storage capacity do not change in the first two cycles, while subsequent cycles decrease the kinetics and the amount of hydrogen absorbed by the sample.

3.2. Surface Analysis. Table 2 gives the atomic concentrations of the different elements in $NaAlH_4$ doped with 5 mol % of Ti on the basis of $TiCl_3$ or Ti_{13}·6THF obtained at different milling times and different absorption/decomposition cycles. Also, Si is present at the surface in samples (a1a), (a1d), (a8a), and (a9d), regardless of whether the precursor used is $TiCl_3$ or Ti_{13}·6THF. This is due to a potential contamination of the material with small amounts of silicon oil (into which the reactor is immersed during the cycling experiments) when the reactor is opened between the cycles to remove the material for the spectroscopic measurements. Apart from the presence of K, B, N, and Br due to the synthesis of the Ti colloid itself,[13] the main contaminants at the surface are carbon and oxygen.

Upon milling the $TiCl_3$ or Ti_{13}·6THF doped samples, the atomic concentration of Ti at the surface is decreasing with increasing milling time. The significant difference between the two precursors is that metallic aluminum is already present at the surface in $TiCl_3$ doped Na-alanate after 2 min of ball milling, whereas it is absent in the case of Ti colloid doped alanate at any milling time. Another difference is the drastic reduction of Ti at the surface in $TiCl_3$ doped samples after 30 min of ball milling compared to the slow decrease in the surface concentration of Ti in Ti colloid doped samples with increasing milling time. In the following section, results obtained for samples (a1a), (a1d), (a8a), and (a9d) with both precursors shall be compared with the corresponding sample, (bm30). The cycling under hydrogen was performed after ball milling of the mixture of Na-alanate and the precursor for 30 min. The surface concentration of carbon increased with the number of cycles in $TiCl_3$

TABLE 2: Atomic Concentrations Obtained from the Study of XPS Surveys of Na-Alanate, $TiCl_3$, Ti_{13}·6THF, and $NaAlH_4$ Doped with 5 mol % of Ti on the Basis of $TiCl_3$ or Ti_{13}·6THF after Different Milling Times and Different Cycles under Hydrogen[a]

	atomic concentration (%)													
sample	C	O	Na	Al	Al^{3+}	Al^0	Ti	Cl	Si	K	B	N	Br	ref
$NaAlH_4$	4.7	32.4	28.1	34.0				0.5	0.3					12
$TiCl_3$		8.4					25.7	65.9						12
Ti_{13}·6THF	46.2	28.0					3.1		18.3	2.0	1.2	1.2		19
$NaAlH_4$ Doped with 5 mol % $TiCl_3$ by Ball Milling														
(bm2)	7.3	32.9	24.9	21.5	**18.1**	**3.4**	2.8	10.6						12
(bm30)	8.4	35.6	25.4	24.7	**20.1**	**4.6**	0.6	5.3						12
(bm60)	9.9	34.6	25.5	25.4	**21.1**	**4.3**	0.5	4.1						12
(bm180)	11.6	36.6	26.2	21.6	**20.2**	**1.4**	0.4	3.6						19
(a1d)	8.3	43.3	26.5	16.0	**12.6**	**3.4**	0.3	4.6	1.0					
(a1a)	9.3	40.7	27.9	16.5	**14.4**	**2.1**	0.4	4.4	0.8					
(a8a)	13.5	40.6	25.0	16.0	**13.8**	**2.2**	0.4	2.8	1.7					
(a9d)	13.1	40.6	25.4	15.9	**11.1**	**4.8**	0.4	3.9	0.7					
$NaAlH_4$ Doped with 5 mol % Ti_{13}·6THF by Ball Milling														
(bm2)	25.9	34.8	13.6	13.5	**13.5**		3.4		6.7	0.8		1.1	0.2	19
(bm30)	20.1	36.6	20.6	16.3	**16.3**		3.0		1.6	0.3		1.2	0.3	19
(bm60)	13.0	41.4	25.4	15.6	**15.6**		2.3		1.0	0.3		0.7	0.3	19
(bm180)	9.3	46.5	27.7	14.3	**14.3**		1.3		0.2	0.2		0.4	0.1	19
(a1d)	8.8	45.8	29.5	12.8	**7.4**	**5.4**	1.7			0.2	0.9	0.3		
(a1a)	9.1	44.1	28.0	16.4	**15.4**	**1.0**	0.8	0.1	0.3		1.1	0.1		
(a8a)	11.9	42.7	33.0	11.2	**9.3**	**1.9**	0.5		0.3			0.4		
(a9d)	23.8	34.6	24.6	12.2	**6.6**	**5.6**	0.6		3.4			0.8		

[a] Samples (a1a), (a1d), (a8a), and (a9d) with both precursors shall be compared with the corresponding sample (bm30).

TABLE 3: XPS Binding Energies (in eV) of the Reference Samples[a]

ref sample	Na 1s	Ti $2p_{3/2}$	O 1s	C 1s	Cl $2p_{3/2}$	Al 2p	Na 2s	ref
Al[b]						72.9		12
Al_2O_3			531.0			74.4		12
AlO(OH)			531.5			74.2		12
Ti[b]		454.0						12
TiH_2		454.6						
TiO_2		458.6	529.8					12
$TiCl_3$		458.5			199.5			12
$TiCl_3$		459.8			*200.7*			12
$TiAl_3$[b]		453.8				72.4		12
$NaAlH_4$	1073.9		**532.7**	*c*	*200.7*	75.4	65.6	12
			534.2					
Ti_{13}·6THF[b] (∼0)		456.1	530.9	286.0				19
(∼I)		457.5	532.0					
(∼III)		**459.3**	**533.7**					

[a] If several values are given, the binding energy of the most intense line is printed in bold. Charge reference lines for isolating samples are shown in italic type. [b] Conductors. [c] The C 1s line superimposed with the plasmon loss line of Cl 2s.

TABLE 4: XPS Binding Energies (in eV) of Doped Na-Alanate after a Milling Time of 30 min and at Different Stages of the Dehydrogenation−Rehydrogenation Reaction[a]

sample	Na1s	Ti $2p_{3/2}$	O 1s	C 1s	Cl $2p_{3/2}$	Al 2p	Na 2s	ref
			$NaAlH_4$ Doped with 5 mol % $TiCl_3$ by Ball Milling					
(bm30)	1073.6 [1.76]	454.2	**531.9**	**287.0**	*200.7* [1.15]	72.8	65.3 [1.53]	12
			533.4	290.8		**75.1 [1.74]**		
(a1d)[b]	1074.0 [2.05]	454.2	**532.6**	**287.5**	201.3 [1.36]	72.7	65.7 [2.07]	
			534.0	290.4		**75.7** [**1.78**]		
				292.1				
(a1a)	1073.4 [2.14]	454.5	**532.6**	**286.6**	201.4 [1.47]	73.0	*65.3* [2.07]	
			534.1	288.6		**75.6** [**1.84**]		
				291.2				
(a8a)[b]	1073.7 [1.88]	454.2	530.5	**287.1**	201.5 [1.46]	72.9	65.4 [1.89]	
			532.5	289.1		**75.5** [**1.72**]		
			533.9	291.5				
(a9d)[b]	1073.6 [1.89]	454.2	531.1	286.0	201.6 [1.58]	72.9	65.1 [1.86]	
			532.7	**287.3**		**75.7** [**1.79**]		
			534.1	288.9				
				291.5				
			$NaAlH_4$ Doped with 5 mol % Ti_{13}·6THF by Ball Milling					
(bm30)[b]	1073.6 [1.84]	456.2	530.7	286.8		75.4 [1.55]	65.5 [1.77]	19
		457.8	**532.1**					
		459.5	533.5					
(a1d)[b]	1073.2 [1.55]	455.2	531.1	286.0		72.7	64.9 [1.49]	
		456.9	**532.7**	**287.2**		**75.2** [**1.80**]		
		459.0	534.3	288.5				
				291.1				
(a1a)[b]	1073.3 [1.77]	455.3	530.8	286.0		72.8	65.1 [1.80]	
		457.0	**532.4**	**287.2**		**75.2** [**1.59**]		
		459.0	533.9	288.5				
				291.1				
(a8a)[b]	1073.2 [1.53]	453.9	530.9	285.9		72.7	64.8 [1.53]	
			532.4	**287.1**		**75.2** [**1.59**]		
			534.0	288.4				
				290.9				
(a9d)[b]	1073.5 [1.59]	453.9	531.1	**286.7**		72.8	65.0 [1.51]	
			532.6	288.3		**75.3** [**1.74**]		
			534.2					

[a] If several values are given, the binding energy of the most intense line is printed in bold. Charge reference lines for isolating samples are shown in italic type. Values of the FWHM are given in eV in square brackets. [b] Conductors.

doped samples, whereas in the case of Ti colloid doped samples it decreased during the first cycle and then increased with an increasing number of cycles. In both cases, the atomic concentration of oxygen at the surface increased with the number of cycles. The evolution of the relative amount of Ti at the surface upon cycling was not significant in the case of $TiCl_3$ doped Na-alanate. From 0.6 at. % in sample (bm30), it decreased and remained at 0.4 at. % between the first and the eighth absorption cycles. In the case of Ti_{13}·6THF doped alanate, however, the concentration of Ti at the surface decreases with an increasing number of hydrogenation/dehydrogenation cycles, from 3.0 at. % in sample (bm30) to 0.6 at. % in sample (a9d). This indicates that after eight cycles the amount of Ti present at the surface is around 0.5 at. %, regardless of whether the precursor used is $TiCl_3$ or Ti colloid. Concerning Al, metallic Al appears at the surface during the decomposition reaction of Ti colloid doped samples. The evolution of the Al^{3+}/Al^0 ratio reflects the transformation taking place. Furthermore, in the case of both precursors, metallic aluminum remains at the surface in samples (a1a) and (a8a), thus confirming that the back reaction from NaH and Al to $NaAlH_4$ is incomplete.[18] At the surface, the atomic concentration of metallic Al evolves with the reaction under hydrogen, while the concentration of Ti tends to reach a constant value upon cycling.

Tables 3 and 4 give the binding energies of elemental lines obtained from reference samples and samples investigated in this work, respectively. Upon milling the $TiCl_3$ doped sample, a partial reduction of $TiCl_3$ already occurs after 2 min of milling

(indicated by the presence of the two binding energies of 459.4 and 454.2 eV) and it is completed after 30 min (presence of the metallic component only).[12] When Ti_{13}·6THF is used as precursor, however, no significant change in the binding energies of Ti $2p_{3/2}$, Al 2p, Na 2s, Na 1s, O 1s, and C 1s is observed, indicating that Ti_{13}·6THF does not chemically react with the Na-alanate during the ball milling process.[19] Upon cycling, the valence state of titanium remains in the metallic state when using the $TiCl_3$ doped Na-alanate, whereas a reduction to the metallic state occurs after the first dehydrogenation−hydrogenation reaction in the Ti colloid sample. After eight cycles, the titanium species are in the zerovalent state, irrespective the precursor used is $TiCl_3$ or Ti_{13}·6THF. Moreover, the binding energies of Al 2p remain at 75.4 and 72.9 eV during the cycles under hydrogen, which correspond to $NaAlH_4$ and metallic Al, respectively. Independently of the precursor used, the binding energies of the Ti $2p_{3/2}$ and O 1s lines of samples (a8a) and (a9d) are similar. The significant difference between these samples results from the binding energy of the Al 2p and Na 2s lines. Comparison of the binding energy differences between the Al 2p line and the Na 2s line displays that the difference is smaller for pure alanate than for samples (a8a) or (a9d). This indicates that the electronic state of Al and Na is more sensitive to the dehydrogenation−rehydrogenation reaction than the one of Ti. Moreover, comparison of the differences between the following lines Na 1s and Na 2s, Al 2p and Na 2s, and Al(3+) 2p and Al(0) 2p of the pure alanate and the Ti colloid or $TiCl_3$ doped samples after 8 absorption cycles suggests that the Na environment is similar, while the Al environment undergoes changes. Furthermore, the binding energies of Al 2p and Na 2s of the Ti colloid doped samples of (a8a) are lower than those of the $TiCl_3$ doped samples of (a8a) or those of pure alanate. This suggests that the surface of Ti colloid doped alanate has a higher electron density than that of the $TiCl_3$ doped Na-alanate.

3.3. Bulk Analysis. Earlier XANES data[10,20] were used to complement the XPS analysis. In the case of $TiCl_3$ doped alanate, Ti species are indeed reduced from Ti^{3+} to Ti^0 during ball milling (a shift in the edge occurs from 4972 eV for $TiCl_3$ to 4966 eV, which corresponds to the metallic Ti) and remain in the metallic state under subsequent hydrogenation−dehydrogenation cycling.[10] In Na-alanate doped with Ti colloid, the valence state of Ti is unchanged upon milling (independently of the milling time, the first inflection point remains at 4967 eV) but a shift to the metallic state occurs during the first hydrogenation cycle (a small shift of the first inflection point to 4966 eV occurs).[20] Then, further cycling does not affect the oxidation state of the Ti in the case of both precursors.

The $TiCl_3$ local structure around the Ti atoms consists of six Cl atoms with d(Ti−Cl) = 2.45 Å.[10] The Ti_{13}·6THF structure consists of a Ti metal core having an icosahedral shape and six THF ligands with d(Ti−O) = 2.02 Å and d(Ti−Ti) = 2.89 Å.[13]

Figure 5 displays the raw EXAFS spectra of samples $TiCl_3$(a8a), $TiCl_3$(a9d), Ti_{13}·6THF(a8a), and Ti_{13}·6THF(a9d) together with the one of metallic Ti, $TiAl_3$, and TiH_2. It can be seen that, after eight cycles under hydrogen, a similar structure is formed, no matter which precursor is used. However, the amplitude of the signal is much more pronounced in samples $TiCl_3$(a8a) and $TiCl_3$(a9d) than in samples Ti_{13}·6THF(a8a) and Ti_{13}·6THF(a9d), indicating that the degree of order around Ti is higher in $TiCl_3$ doped samples than in Ti colloid doped samples. A comparison of these spectra with the reference samples suggests that in both cases the local structure is the crystalline structure of neither Ti, TiH_2, nor exactly $TiAl_3$ (significant differences in the fine structure are obvious from the EXAFS signals of the Ti-based precursor and crystalline $TiAl_3$). Nevertheless, the amplitude of EXAFS signals of the Ti-based precursor are only in phase with the signal from the $TiAl_3$ spectrum.

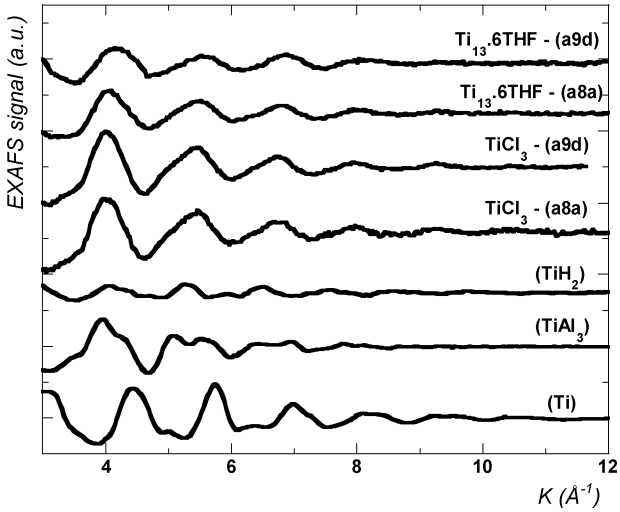

Figure 5. EXAFS spectra $\chi(k)$ of Ti, $TiAl_3$, TiH_2, and Na-alanate doped with 5 mol % of Ti on the basis of $TiCl_3$ or Ti_{13}.6THF after eight absorption cycles (for sample (a8a)) and subsequent desorption (for sample (a9d)).

Figure 6 displays the magnitude of the k^3-weighted Fourier transform (FT) of the EXAFS $\chi(k)$ function of $TiCl_3$ doped Na-alanate (Figure 6a) and Ti_{13}·6THF doped samples (Figure 6b) that have been ball milled for 30 min, at different stages of the dehydrogenation−reydrogenation reaction. Figure 6a exhibits a one-shell structure with a shift of the main peak from 1.99 Å in pure $TiCl_3$ to 2.39 Å (uncorrected for phase shifts) in samples (da) and (a8a), indicating that a new local structure is formed upon cycling under hydrogen. A comparison of the intensities of the signal in samples (da) and (a8a) suggests that the number of backscatterers and/or the order within the first shell of the neighbors increases with the number of cycles under hydrogen. Figure 6b indicates that in Ti colloid doped alanate an evolution occurs from a two-shell to a one-shell structure upon cycling under hydrogen. In the pure colloid sample, Ti_{13}·6THF, the resonances at 1.65 and 2.5 Å represent backscattering from O (THF) and Ti atoms, respectively. In EXAFS analysis, this corresponds to a Ti−Ti distance of 2.86 ± 0.02 Å and a Ti−O distance of 2.03 ± 0.02 Å which is in accordance with results published earlier.[13] In samples (da) and (a2a), the intensity of the oxygen peak decreases, indicating that the number of O atoms around Ti is reduced during the first cycles under hydrogen. After eight cycles, only one intense peak is present, suggesting that the O atoms are completely stripped off from the Ti metallic core. The intensity of the peak in sample (a8a) is more pronounced compared to all the other samples, indicating that the number and/or order of next neighbors also increases with the cycles in this case.

EXAFS data fit analysis was carried out on samples (a8a) of Na-alanate doped with $TiCl_3$ or Ti colloid. Table 5 presents the metric parameters obtained from the least-squares fitting for $TiCl_3$ and Ti colloid doped alanate. Figure 7a represents the magnitude and imaginary part of the Fourier transform as well as the fit in R space of the samples of Ti_{13}·6THF (a8a). Figure 7b displays the corresponding Fourier-filtered data and the fit in k-space. In the $TiCl_3$ doped sample, an evolution occurs upon cycling under hydrogen from a distorted hcp structure with Ti−Ti distances of 2.84 and 3.0 Å to a structure consisting of Al and Ti backscatterers. In samples (a8a) and (a9d), the first Al

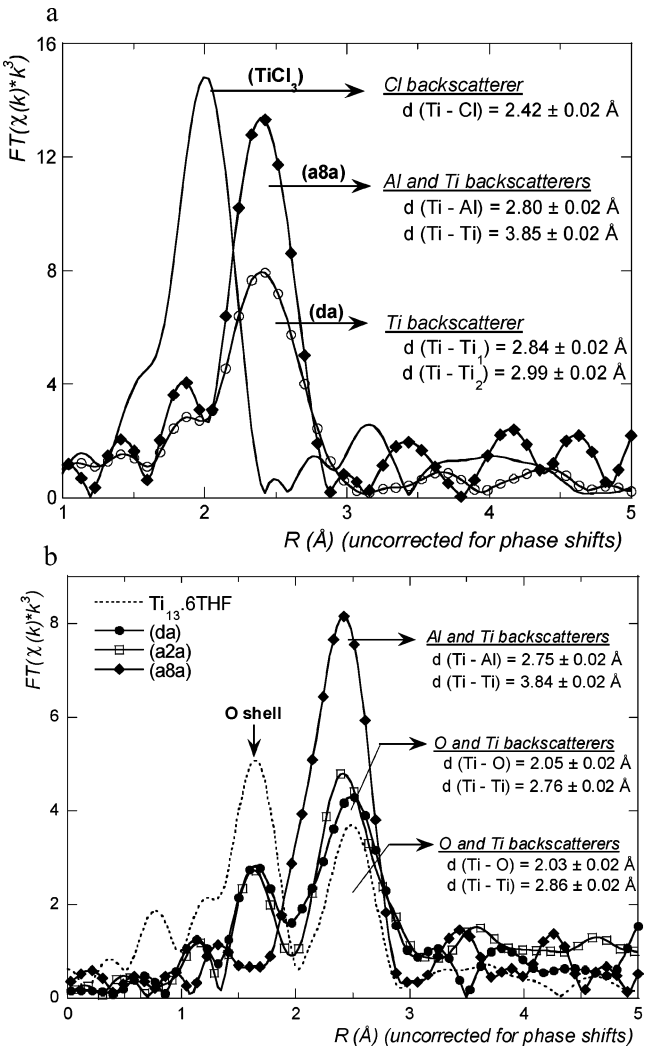

Figure 6. (a) Fourier transform of the k^3-weighted $\chi(k)$ function of sodium alanate doped with 5 mol % of Ti on the basis of $TiCl_3$ at different stages of the dehydrogenation−rehydrogenation reaction. (b) Samples doped with 5 mol % of Ti on the basis of Ti_{13}.6THF.

neighbor shell relaxes into a single distance coordination sphere (Ti−Al distance of 2.8 Å) only compared to the bulk $TiAl_3$ (Ti−Al distances of 2.72 and 2.88 Å). Samples $TiCl_3$(a8a), $TiCl_3$(a9d), and Ti_{13}·6THF(a8a) are rather similar, but the local structure is more distorted in the case of Ti colloid doped samples compared to that of the $TiCl_3$ doped ones.

4. Development on the Local Structure around Ti Atoms

4.1. Evolution of the Local Structure around Ti. In the case of $TiCl_3$ doped alanate, the local structure is evolving from a distorted hcp structure with Ti−Ti distances of 2.84 and 3.0 Å[10] during the first cycle to a structure exhibiting Al and Ti backscatterers after eight cycles. According to EXAFS, the intermetallic phase consists of 10 Al atoms in the first shell with an interatomic distance of 2.80 ± 0.02 Å and about 1 Ti atom in the second shell with an interatomic distance of 3.88 ± 0.02 Å. The significant reduction of the Ti coordination number and the relaxation to a single distance compared to the $TiAl_3$ with tetragonal symmetry (four Al atoms at 2.72 Å, eight Al atoms at 2.88 Å, and four Ti atoms at 3.85 Å) indicates the formation of a very small entity upon cycling under hydrogen.

In the case of the Ti colloid doped sample, the local structure turns from a two-shell structure (O and Ti backscatters) during the first cycles to a one-shell structure by stripping off the THF oxygen atoms from the metallic core. After eight cycles, the local structure consists of a structure similar to that of $TiCl_3$ doped sample with nine Al atoms at 2.75 ± 0.02 Å and one Ti atom at 3.84 ± 0.02 Å.

In the case of both Ti-based precursors, an evolution of the local structure around Ti atoms occurs upon cycling under hydrogen. Even though the changes are different during the first cycling under hydrogen, a similar cluster is formed in both cases after eight dehydrogenation−rehydrogenation cycles. Significant differences in the EXAFS fine structure and the lack of long-range order indicate that this local structure (10 Al atoms at 2.80 ± 0.02 Å and 1 Ti atom at 3.88 Å) does not exactly correspond to the $TiAl_3$ bulk phase.

The local Ti environment observed for the $TiCl_3$ doped sample after several cycles is in agreement with data published recently.[21] In our opinion, this local structure is more plausible than the one suggested by another study,[8] where 17 atoms were proposed within a range of 3 Å. The former results[21] and our own findings suggest that the formation of an intermetallic phase between Al and Ti is independent of the milling parameters. It already evolves after 4 cycles[8,21] under hydrogen and remains during subsequent cycling. Moreover, the formation of small Ti/Al entities would explain why this phase was not detected by XRD[2,3] or TEM[8,9] techniques.

4.2. Location of the Ti−Al Cluster. The experimental setup used in the different EXAFS studies (transmission mode[8] and fluorescence mode with samples oriented to have the incident beam at 45°[10,11]) results in the penetration depth of the X-rays into the material being in the micrometer range. Thus, the information obtained from these measurements reflects the local structure of the bulk material. In contrast to this, the XPS technique is surface sensitive (in the nanometer range for the samples studied herein). Analysis of the atomic concentration and the binding energies presented in this work indicates that $TiAl_3$ alloy, TiO_2, TiH_2, or Al_2O_3 are not present at the surface of the samples. However, the presence of the particular local structure between Ti and Al at the surface cannot be excluded strictly by XPS.

4.3. Evolution of the Kinetics with the Formation of a Ti−Al Cluster. According to XPS analysis, the fastest kinetics are observed for Ti colloid doped samples having the lowest concentration of Ti at the surface after ball milling. Concerning the storage capacity, 5.5 wt % of H_2 is released from sample (bm2), (bm30), or (bm180) after the first decomposition, suggesting that the hydrogen capacity is likely independent of the surface concentration of Ti. This result can probably be correlated with the fact that, upon milling, the Ti colloid does not react chemically with the sodium alanate (the binding energy of Ti $2p_{3/2}$ and the local structure around Ti atoms are unchanged irrespective of the milling time, and metallic Al is absent at the surface). In the subsequent cycles, however, the kinetics and the storage capacity decrease. Moreover, the two decomposition steps cannot be distinguished in the first cycle, while the second desorption step is more pronounced from the second cycle. According to XPS and XAS analysis, oxygen atoms are stripped off from the Ti core and a shift to the Ti metallic state occurs during the first cycle. At a certain point, the presence of metallic Ti and metallic Al favors the formation of an intermetallic phase. Formation of the Ti−Al cluster eliminates a fraction of Al, and thus, the incomplete back reaction would explain why the reversible hydrogen storage capacity decreases during the first cycles and then stabilizes around 4.5 wt % after 4 cycles.

The concentration of Ti at the surface tends to already be constant after the first cycle and is nearly invariant during

TABLE 5: Data Range and Metric Parameters Obtained by EXAFS Least-Square Fits for $TiCl_3$ and Ti_{13}·6THF Doped Na-Alanate at Different Stages of the Dehydrogenation−Rehydrogenation Reaction[a]

sample labels	fit range $R-\Delta$ (Å)	shell	R (Å) (±0.02 Å)	N (±0.2)	σ^2 (Å^2)	ΔE (eV)	R-factor
		$NaAlH_4$ Doped with 5 mol % $TiCl_3$ by Ball Milling					
$TiCl_3$[c]	1.25−2.62	Cl	2.42	5.9	0.0028	5.3	0.02
(dd)[c]	1.65−2.91	Ti_1	2.84	2.9[b]	0.0056	−6.7[b]	0.03
		Ti_2	3.00	2.9[b]	0.0049	−6.7[b]	
(da)[c]	1.36−2.91	Ti_1	2.84	5.3[b]	0.0050	−9.2[b]	0.008
		Ti_2	2.99	5.3[b]	0.0042	−9.2[b]	
(a8a)	2.02−3.71	Al	2.80	10.7	0.0057	5.9	0.009
		Ti	3.85	0.8	0.0002	−2.2	
(a9d)	1.90−3.74	Al	2.80	11.9	0.0075	6.0	0.008
		Ti	3.88	1.9	0.0065	−1.7	
		$NaAlH_4$ Doped with 5 mol % Ti_{13}·6THF by Ball Milling					
Ti_{13}·6THF	1.31−2.88	O	2.03	2.9	0.0050	13.3	0.001
		Ti	2.86	2.2	0.0075	6.3	
(da)	1.32−2.94	O	2.05	1.2	0.006	13.0	0.016
		Ti	2.76	4.3	0.001	−12.8	
(a8a)	1.93−3.71	Al	2.75	8.37	0.0078	5.128	0.015
		Ti	3.84	1.0	0.0032	0.219	

[a] S_0^2 was fixed at 1 for Ti_{13}·6THF and 0.6 for all the other samples. [b] Denotes that fit parameters are forced to be equal for both shells. [c] Results published in ref 21.

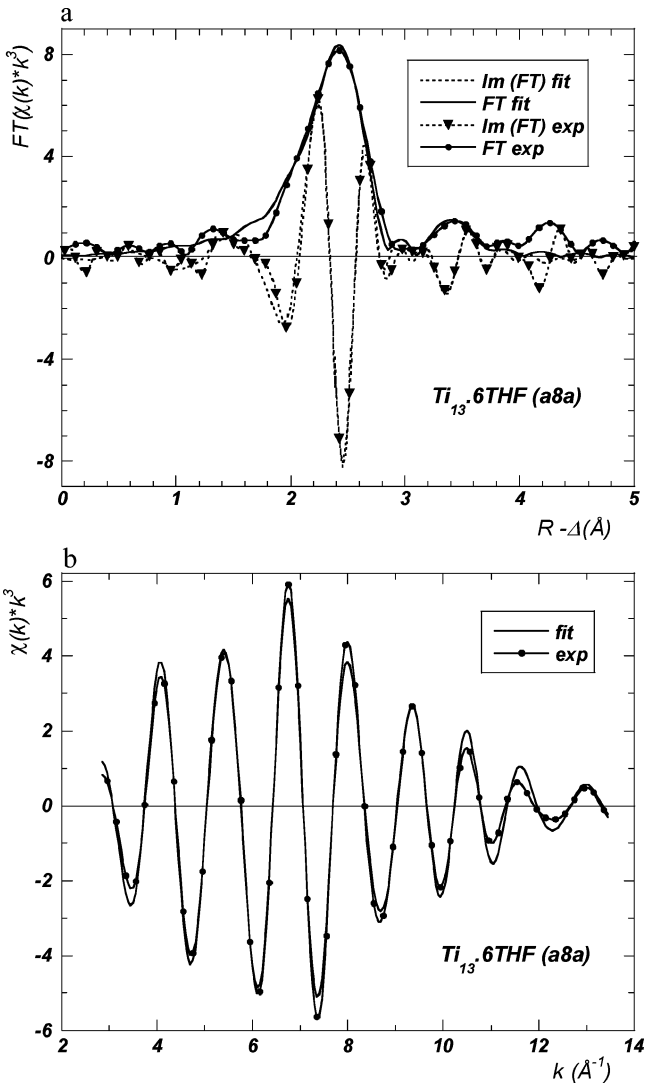

Figure 7. (a) FT magnitude and imaginary part, R-space fit magnitude, and imaginary part of the Ti_{13}·6THF(a8a). (b) Fourier-filtered data and fit in k-space.

hydrogen cycling. In contrast to this, the concentration of Al(0) at the surface varies significantly with dehydrogenation and subsequent hydrogenation (for example, for Ti colloid doped Na-alanate, we have 5.4 at. % in sample (a1d) and 1.0 at. % in sample (a1a)). This indicates that the metallic Al phase migrates under hydrogen cycling, whereas the metallic Ti phase does not segregate. A detailed analysis of the kinetics of absorption and decomposition data also showed that a diffusion like growth process most likely governs the phase transformations in Ti doped $NaAlH_4$.[13,14]

5. Conclusion

This combined study indicates that the significant difference between the two precursors used in this study is that $TiCl_3$ already reacts chemically with the alanate after 2 min of ball milling, whereas Ti_{13}·6THF reacts with the Na-alanate during the first rehydrogenation cycle only. Moreover, the atomic concentration of metallic titanium at the surface during cycling under hydrogen tends to a constant value of 0.5 at. % in both cases, whereas the atomic concentration of metallic Al at the surface changes with the desorption and absorption of hydrogen. Analysis of the binding energies reveals that, at the surface, the Al and Na lines are more sensitive to the dehydrogenation−rehydrogenation reaction than the Ti line. Moreover, the O, Na, and Ti environment is similar after eight cycles in both cases, while the Al environment undergoes changes. Additionally, the surface of Ti colloid doped alanate has a higher electron density than that of the $TiCl_3$ doped Na-alanate. Furthermore, the Ti species do not remain at the surface upon milling and subsequent cycling, irrespective of the Ti-based precursor used to activate the reversible decomposition reaction of Na-alanate. Upon cycling under hydrogen, the local structure around Ti atoms first evolves differently for $TiCl_3$ or Ti colloid doped samples. After several cycles, however, a particular local arrangement consisting of 10 Al atoms in the first shell with an interatomic distance of 2.80 ± 0.02 Å and a small but significant Ti contribution in the second shell (about 1 Ti atom at 3.88 ± 0.02 Å) is formed, regardless of the nature of the precursor used. The formation of this Ti−Al cluster as well as the incomplete back reaction seems to be responsible for the decrease of the reversible hydrogen storage capacity during the first hydrogenation−dehydrogenation cycles. The decrease of the desorption−absorption reaction rate is correlated with the formation of this local structure.

Acknowledgment. Financial support by the EU-SP STORHY Contract Number 502667 is gratefully acknowledged. We appreciate beam-time allotment by ANKA and the experimental

assistance by Stefan Mangold and the ANKA-ISS staff. Christoph Frommen and Stephan Wetterauer are gratefully acknowledged for their support in chemical synthesis and sample preparation.

References and Notes

(1) Bogdanovic, B.; Schwickardi, M. *J. Alloys Compd.* **1997**, *253*−*254*, 1.

(2) Gross, K. J.; Sandrock, G.; Thomas, G. *J. Alloys Compd.* **2002**, *330*−*322*, 691.

(3) Weidenthaler, C.; Pommerin, A.; Felderhoff, M.; Bogdanovic, B.; Schüth, F. *Phys. Chem. Chem. Phys.* **2003**, *5*, 5149.

(4) Hauback, B. C.; Brinks, H. W.; Jensen, C. M.; Murphy, K.; Maeland, A. J. *J. Alloys Compd.* **2003**, *358*, 142.

(5) Ozolins, V.; Majzoub, E. H.; Udovic, T. J. *J. Alloys Compd*. **2004**, *375*, 1.

(6) Bogdanovic, B.; Brand, R. A.; Marjanovic, A.; Schwickardi, M.; Tölle, J. *J. Alloys Compd.* **2000**, *302*, 36.

(7) Thomas, G. J.; Gross, K.; Yang, N. Y. C.; Jensen, C. *J. Alloys Compd.* **2002**, *330*−*332*, 702.

(8) Felderhoff, M.; Klementiev, K.; Grünert, W.; Spielthoff, B.; Tesche, B.; Bellosta von Colbe, J. M.; Bogdanovic, B.; Härtel, M.; Pommerin, A.; Schüth, F.; Weidenthaler, C. *Phys. Chem. Chem. Phys.* **2004**, *6*, 4369.

(9) Léon, A.; Kircher, O.; Rösner, H.; Décamps, B.; Leroy, E.; Fichtner, M.; Percheron-Guégan, A. *J. Alloys Compd.* **2005**, available online.

(10) Léon, A.; Kircher, O.; Rothe, J.; Fichtner, M. *J. Phys. Chem. B* **2004**, *108*, 16372.

(11) Graetz, J.; Reilly, J. J.; Johnson, J.; Ignatov, A. Y.; Tyson, T. A. *Appl. Phys. Lett.* **2004**, *85*, 500.

(12) Léon, A.; Schild, D.; Fichtner, M. *J. Alloys Compd.* **2005**, *404*−*406*, 766.

(13) Fichtner, M.; Fuhr, O.; Kircher, O.; Rothe, J. *Nanotechnology* **2003**, *14*, 778.

(14) Kircher, O.; Fichtner, M. *J. Appl. Phys.* **2004**, *95*, 7748.

(15) Sayers, D. E.; Bunker, B. A. In *X-ray Absorption: Techniques of EXAFS, SEXAFS and XANES*; Koningsberger, D. C., Prins, R., Eds.; Wiley: New York, 1988; pp 211−253.

(16) Stern, A. E.; Newville, M.; Ravel, B.; Yacoby, Y.; Haskel, D. *Physica B* **1995**, *208*−*209*, 117.

(17) Seah, M. P.; Gilmore, I. S.; Beamson, G. *Surf. Interface Anal.* **1998**, *26*, 642.

(18) Bogdanovic, B.; Felderhoff, M.; German, M.; Härtel, M.; Pommerin, A.; Schüth, F.; Weidenthaler, C.; Zibrowius, B. *J. Alloys Compd.* **2003**, *350*, 246.

(19) Léon, A.; Rothe, J.; Schild, D.; Fichtner, M. *Chem. Eng. Trans.* **2005**, *8*, 171.

(20) Léon, A.; Kircher, O.; Rothe, J.; Fichtner, M. *J. Metastable Nanocryst. Mater.* **2005**, *24*−*25*, 319.

(21) Graetz, J.; Ignatov, A. Y.; Tyson, T. A.; Reilly, J. J.; Johnson, J. *Mater. Res. Soc. Symp. Proc.* **2005**, *837*.